ATLAS Internal Note
INDET-NO-099
27 February 1995

Tau Identification in the ATLAS Inner Tracker

P. Luthaus*, G. Stavropoulos*, E. Tsesmelis†

February 27, 1995

Abstract

We study the question of single τ identification in the barrel region of the ATLAS Inner Tracker based on fully simulated hadronic τ decays using various subdetector configurations and track reconstruction algorithms. Particular emphasis is placed on the pattern recognition, momentum resolution and on the measurement of the impact parameter. A τ identification study on a sample of $A^0 \rightarrow \tau\tau$ events in the barrel and end-cap regions of the Inner Tracker is also presented.

*Universität Dortmund
†CERN/PPE

Contents

1 Introduction

Tau identification, particularly at low luminosities, is one of the stated goals of ATLAS. In this note we study the capability of the ATLAS Inner Tracker (IT) to identify τ 's .

The correct identification of τ 's from the potentially very large jet background is very important in providing indicative signals for new processes. At the LHC the capability to efficiently detect final state τ 's is crucial in discovering and making precision measurements of the decays

- $A^0/H^0 \rightarrow \tau\tau$ and
- $t \rightarrow bH^{\pm} \rightarrow \tau\nu_{\tau}$.

The format of this paper is as follows : in section 2 a description of the event and detector simulation is given. Section 3 describes the track reconstruction algorithms used. In section 4 the results on the pattern recognition and momentum measurement based on fully simulated single τ 's are detailed while the $A^0 \rightarrow \tau\tau$ study is presented in section 5. Our conclusions are given in section 6.

2 Event and Detector Simulation

The ATLAS detector is simulated using the standard ATLAS datacards including the full liquid argon calorimetry preceded by the solenoidal coil. The two IT lay-outs studied are those based on the Coseners House and Panel geometries. The primary differences are (a) the inclusion of the large-pad SIT layer in the barrel at a radius of 1 m (outside the TRT) in the latter and (b) all strips in the Panel geometry cross at 90° whereas the Coseners House layers at radii 20 and 30 cm have a narrow stereo angle. It should be noted that neither IT configuration includes a microstrip layer at a radius of 6 cm which would have enhanced the sensitivity to long-lived particles such as τ 's and B's.

For the $A^0 \rightarrow \tau\tau$ study only the Panel geometry is used. In the forward region of the IT there are only microstrip layers without the inclusion of any pixel or pad layers.

The detector simulation of the geometries described above has been performed within the GEANT 3.21 [1] framework. The GEANT routines transport particles through the detector, simulating decays and interactions with the material including conversions, bremsstrahlung, multiple scattering and delta rays. When a charged particle crosses an active layer, the amount $\frac{dE}{dx}$ of energy deposited is recorded in raw data banks. At present the effects of noise and charge sharing from the 2 T solenoidal magnetic field and diffusion have not been included in the silicon detectors.

Single τ datasets have been generated with PYTHIA 5.7 and JETSET 7.3 [2] for each geometrical scenario using the DICE/SLUG/GEANT packages. The DICE/SLUG [3] framework performs the general tasks of providing an

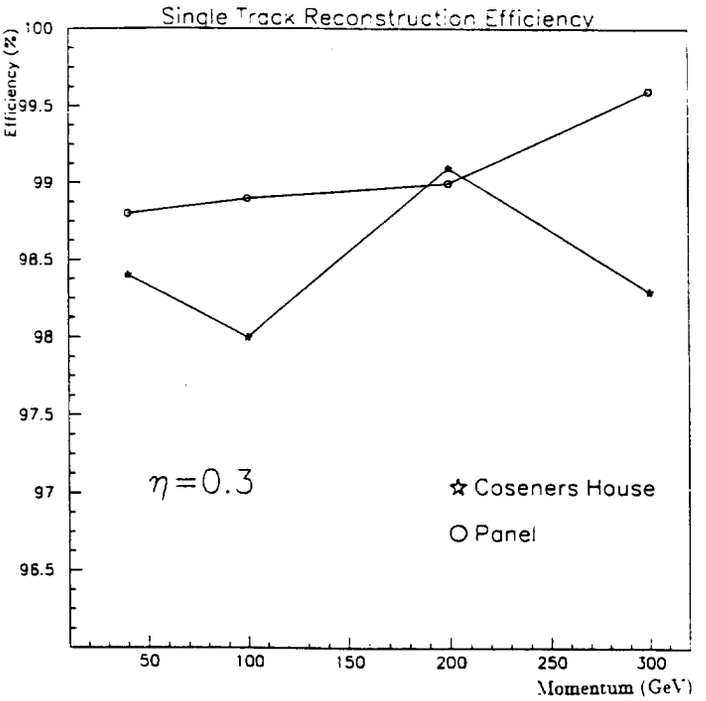

Figure 1: Single track reconstruction efficiency.

interface to GEANT, of the generator event handling and selection of particles to simulate, of providing a flexible structure within which different sets of sub-detectors can be studied together, and of memory management.

The simulated momenta are 40, 100, 200 and 300 GeV generated at η of 0.1, 0.3, and 0.6 over the full azimuthal angular coverage. For every momentum and η combination 1000 single τ 's have been produced separately for the one- and three- prong hadronic τ decay channels.

In addition, a dataset of 989 $A^0 \rightarrow \tau\tau$ (276 events with $m_{A^0} = 150$ GeV, 261 events with $m_{A^0} = 200$ GeV and 452 events with $m_{A^0} = 300$ GeV), events in the lepton-hadron channel have been produced in Dortmund with PYTHIA 5.7 and JETSET 7.3. For the hadronic part only one- and three-prong decays are allowed. Only generated tracks within $|\eta| \leq 3$ are then put into the detector simulation. These events are used to study the IT τ identification capabilities for a complete physics event.

3 The Track Reconstruction Algorithms

Two track reconstruction algorithms are used - each based on distinct philosophies for pattern recognition and track reconstruction.

The first one [4] performs a global pattern recognition in the TRT and as a second step extrapolates the candidate track segments to the barrel SCT and matches them with the silicon hits using the Kalman Filtering method. (It should be noted that the version of the algorithm used was that at its early

stage and since then improvements have been made especially to its pattern recognition capabilities).

In the second one [5], reconstruction is restricted within roads joining the vertex region to 'trigger' seeds. The version of the program used takes its seed from the calorimeter jets (combined information from the electromagnetic and hadronic calorimeters) and reconstructs tracks from the digitizations in the barrel SCT. Since this method does not use information from the TRT, a direct comparison between the pattern recognition capabilities of the TRT and the SCT can be made. For the $A^0 \rightarrow \tau\tau$ study only this second algorithm is used.

For the vertex reconstruction the DELPHI algorithms [6] are adapted in the second algorithm.

4 Track Reconstruction

4.1 Single-prong Hadronic τ Decays

The study for the single-prong hadronic τ decay has been performed using only the second track reconstruction algorithm.

4.1.1 Track Reconstruction Efficiency

Figure 1 summarizes the single track reconstruction efficiencies for the one-prong hadronic τ decays for $\eta = 0.3$. The statistical error on each point is $\pm 0.4\%$. No active layer inefficiency has been included but an additional $\sim 1.5\%$ inefficiency in the track reconstruction is expected from the silicon layer inefficiency. These results are independent of η in the barrel region as has been shown by the similar results obtained for $\eta = 0.1$ and 0.6.

A similar reconstruction efficiency is obtained with either of the IT lay-outs. However, a slight improvement in the mean efficiency is consistently seen for the Panel geometry which can be attributed to the more compact silicon tracker which results in less ambiguities and to the difference in silicon crystal lengths (6 cm for the Panel and 12 cm for the Coseners House geometries, respectively) thus making more difficult the space point reconstruction in the latter case.

In addition, it is possible to evaluate the fake track rate which is the sum of all reconstructed tracks greater than one in the event. The fake tracks are produced artificially by the track reconstruction algorithm since nominally there is only one hadron track from the single τ . In all geometries and for all incident momenta and η 's the fake track rate is $\leq 1.5\%$.

It is also possible to calculate the occurrence rate of the reconstruction algorithm fitting a track of the opposite curvature to the initial particle. Such instances of particle charge misidentification occur up to the $\sim 1\%$ level depending on the momentum.

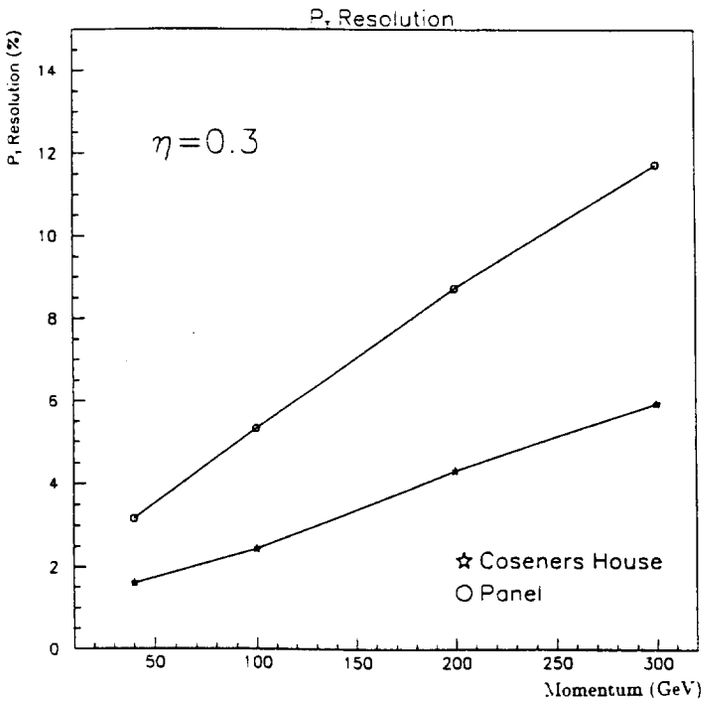

Figure 2: Single track P_T resolution.

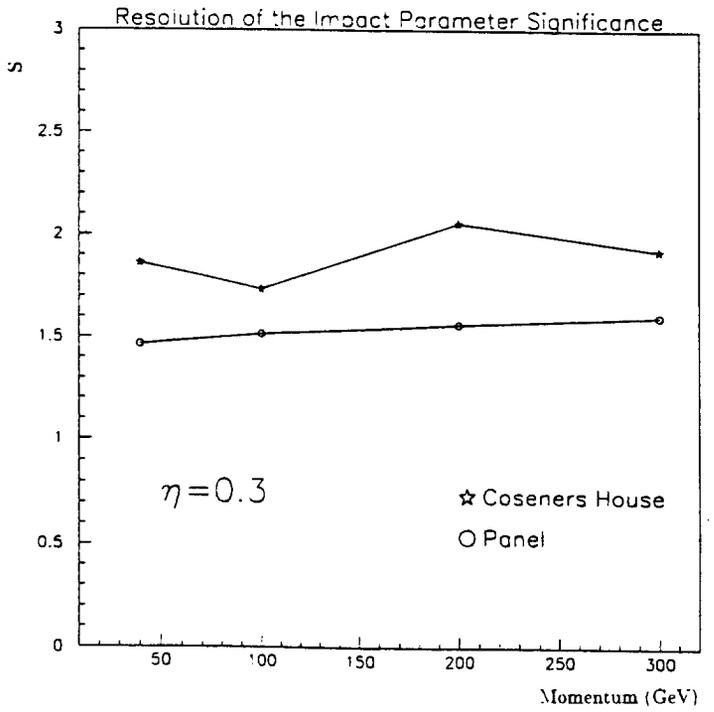

Figure 3: The impact parameter significance.

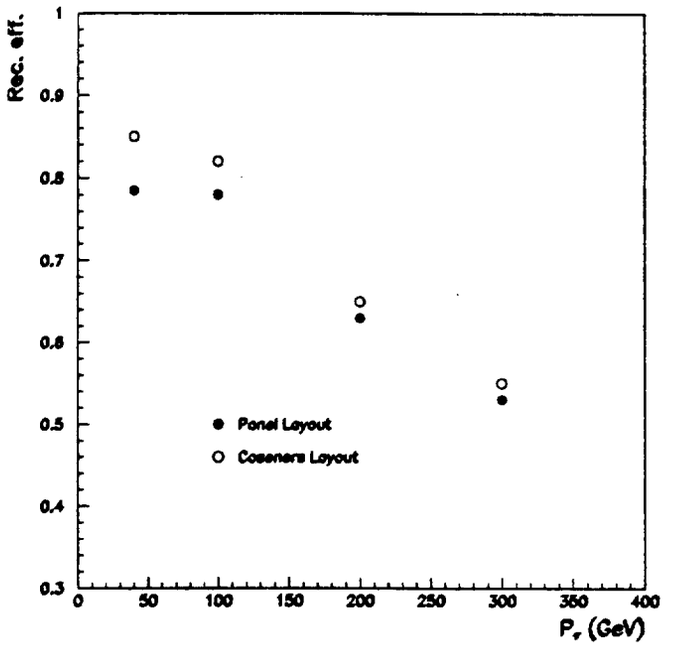

Figure 4: Three track reconstruction efficiency for the Coseners House and Panel lay-outs as a function of the τ momentum using the first reconstruction algorithm.

4.1.2 Transverse Momentum Resolution

The transverse momentum (P_T) resolution for incident τ 's at $\eta = 0.3$ is shown in Figure 2. The resolution is the rms of the Gaussian fit to the ratio of the P_T from the track fit and the nominal P_T . As expected the P_T resolution increases with increasing incident momenta. The resolutions are found to be independent of η in the barrel region as has been checked for $\eta = 0.1$ and 0.6.

The Coseners House geometry gives the better P_T resolution. The measurement of the P_T is superior for such a tracker because it has a silicon strip layer just before the calorimeter thus increasing the radial lever arm for the momentum measurement.

4.1.3 Impact Parameter

As a potential cut against the jet background, we have investigated the impact parameter significance defined as

$$S \equiv \frac{IP}{\sigma_{IP}}$$

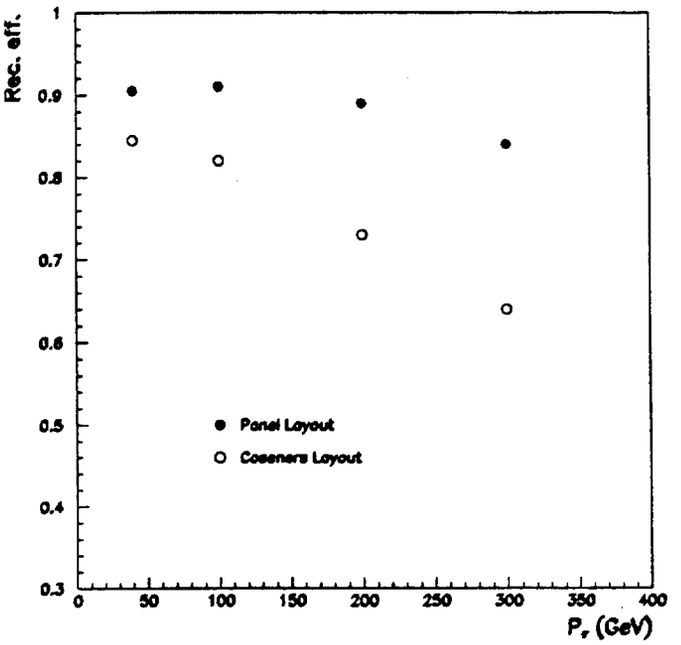

Figure 5: Three track reconstruction efficiency for the Coseners House and Panel lay-outs as a function of the τ momentum using the second reconstruction algorithm.

where IP is the impact parameter. Figure 3 shows the variation of S with incident τ momentum for $\eta = 0.3$. These results are also found to be independent of η in the barrel region.

Therefore, independently of the incident τ momentum, S is slightly higher for the Coseners House geometry. This is because the Coseners House geometry includes two pixel layers (at radii 11.5 and 14.5 cm) while the Panel geometry has only one pixel layer (at radius 11.5 cm). The extra pixel layer in the former case enhances the sensitivity to the secondary vertex of the τ decay. However, S for τ 's is similar to that found in a separate study for the jet background[1] and thus its use to separate τ 's from the jet background is marginal. The evaluation of the impact parameter should be resumed with the inclusion of a microstrip layer at a radius of about 6 cm as suggested for the B-physics studies.

[1]Private communication with D. Cavalli and L. Perini.

4.2 Three-prong Hadronic τ Decays

4.2.1 Track Reconstruction Efficiency

Figures 4 and 5 summarize the three track reconstruction efficiencies, by plotting the percentage of the events where three and only three tracks were reconstructed.

Figure 4 shows the results from the first reconstruction algorithm for the Coseners House and Panel lay-outs for the various τ momenta. The Coseners House lay-out shows a slightly better performance, due to the larger TRT. The results are averaged over the full barrel since no dependence on η was found.

In Figure 5 the same results are shown for the second reconstruction algorithm. The difference observed between the two lay-outs is due to the more compact silicon tracker and shorter silicon crystals in the case of the Panel geometry. The three track reconstruction efficiency with the Panel geometry may be further improved by including narrow stereo strips since they would reduce inefficiencies arising from the two-track separation ambiguities at high momenta.

By comparing Figures 4 and 5 for the Panel lay-out, we conclude that the silicon tracker offers unique capabilities on the reconstruction of nearby space tracks, such as those coming from τ decays.

Figure 6 uses the second algorithm together with the Panel lay-out, in order to estimate the track reconstruction efficiency without the presence of the SIT layer at $R \simeq 1\ m$. By comparing this figure with Figure 5 we conclude that this SIT layer does not contribute significantly to the track pattern recognition.

Figures 7 and 8 show the percentage of the events with more than three reconstructed tracks for both lay-outs and for both reconstruction algorithms as a function of the τ momentum, giving thus the fake track rate. On this aspect the two lay-outs look quite similar, but a small difference is exhibited between the two reconstruction algorithms.

Figure 9 shows the percentage of the events where the τ charge is misidentified for the Panel lay-out and for both reconstruction algorithms. The charge misidentification occurs at the $< 1\%$ level for the second reconstruction algorithm and increases up to $\sim 2\%$ for the first one. The Coseners House lay-out exhibits a similar behaviour.

4.2.2 Transverse Momentum Resolution

The P_T resolution for the Panel lay-out is shown in Figures 10 and 11 for the two reconstruction algorithms. Only the events with exactly three reconstructed tracks are used from the 100 GeV τ sample at η =0.3. Each event enters the histogram three times. The resolution is the σ of the Gaussian fit to the ratio of the reconstructed P_T to the nominal one. The much better resolution that the first reconstruction algorithm achieves is because the full tracker is used (TRT+SCT) whereas only the SCT is used in the second reconstruction

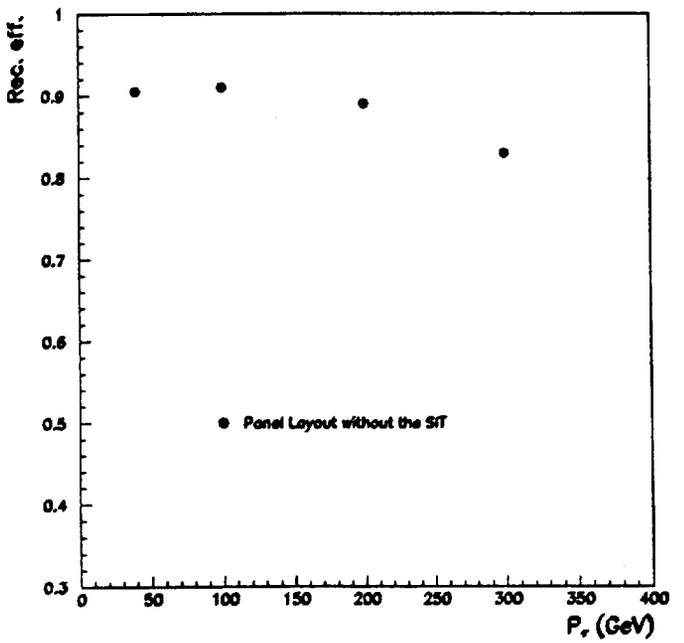

Figure 6: Three track reconstruction efficiency using the Panel lay-out without the outermost SCT layer as a function of the τ momentum.

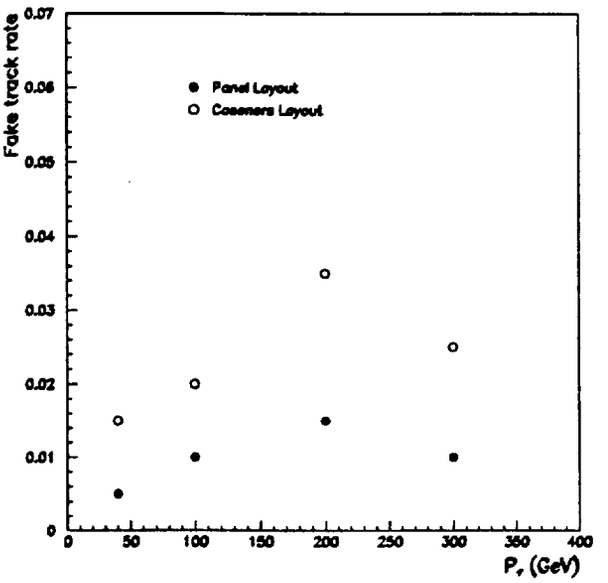

Figure 7: Fake track rate using the first reconstruction algorithm, as a function of the τ momentum.

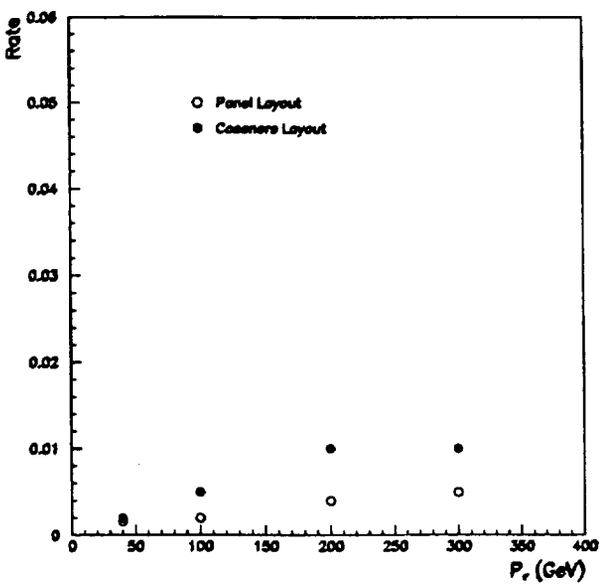

Figure 8: Fake track rate using the second reconstruction algorithm, as a function of the τ momentum.

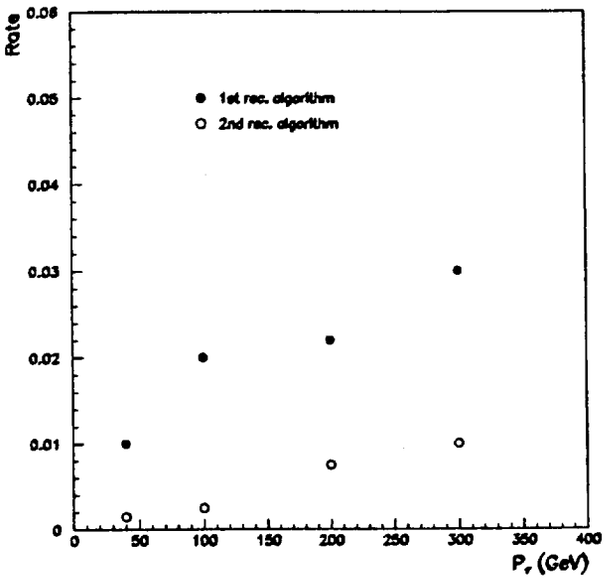

Figure 9: τ charge misidentification rate for the Panel lay-out using both reconstruction algorithms as a function of the τ momentum.

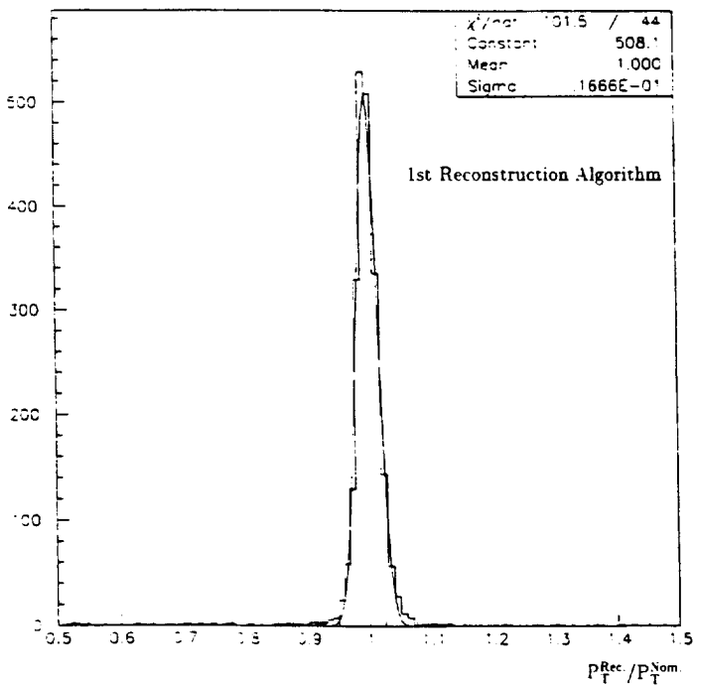

Figure 10: Transverse momentum resolution for the Panel lay-out using the first reconstruction algorithm.

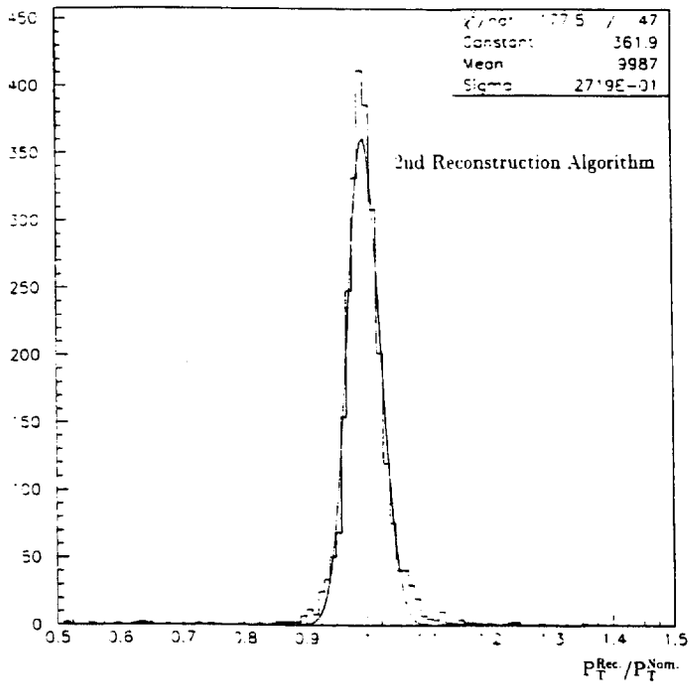

Figure 11: Transverse momentum resolution for the Panel lay-out using the second reconstruction algorithm.

algorithm. The resolution increases with increasing incident momenta and it independent of η . The Coseners House lay-out exhibits a similar behaviour.

4.2.3 τ Decay Vertex Reconstruction

As was mentioned in Section 3, the DELPHI Vertex Reconstruction algorithms were used, suitably adjusted to the second reconstruction algorithm. In Figure 12 the transverse τ decay vertex resolution is plotted versus the τ incident momenta. The resolution is the σ of the Gaussian fit to the reconstructed transverse τ decay vertex. The results shown in this plot are expected to improve significantly when the whole tracker (including the TRT) are included in the track reconstruction and when a microstrip layer is added at a small radius. The Coseners House lay-out exhibits a similar behaviour.

5 $A^0 \rightarrow \tau\tau$ study

5.1 Track Reconstruction Efficiency

Using the $A^0 \rightarrow \tau\tau$ events mentioned in Section 2, the track reconstruction efficiency was studied in the barrel and end-cap regions of the Panel IT using the second reconstruction algorithm. In the events where the τ decayed into one-prong the track reconstruction efficiency is similar (within errors) for the

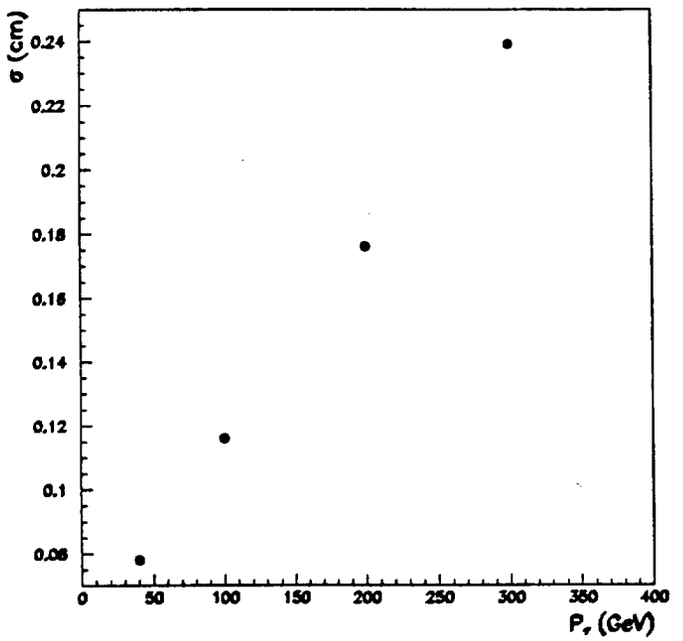

Figure 12: Transverse τ decay vertex resolution for the Panel lay-out.

barrel and end-cap regions. Namely, in $(91 \pm 3)\%$ of the one-prong events the track coming from the τ was reconstructed.

However, this is not the case for the three-prong τ decays. In the barrel region the efficiency to reconstruct all three tracks is $(84 \pm 4)\%$ whereas for the end-cap region it is only $(68 \pm 5)\%$. A similar behaviour is observed for the charge misidentification for three-prong τ decays. In the barrel region the charge misidentification rate is $(1.8 \pm 0.1)\%$ but rises to $(5.0 \pm 2.0)\%$ in the end-cap. This is because in the end-cap region of the Panel lay-out each track has less than six measured points, thus deteriorating the pattern recognition performance of the detector. In addition, the results from the barrel region show that pixel layers are important for the pattern recogniton since they would aid in reducing inefficiencies from (a) losses due to jets opening up, (b) lack of two-track resolution at high momenta and (c) low energy tracks leaving the trigger road. The inclusion of pixel or pad layers in the forward region should thus facilitate an improved pattern recognition.

5.2 Transverse Momentum Resolution

Figures 13 and 14 show the ratio of the P_T from the track fit to the nominal P_T for the barrel and end-cap regions, respectively. The significantly different σ values of the Gaussian fits demonstrate the difference of the performance. This

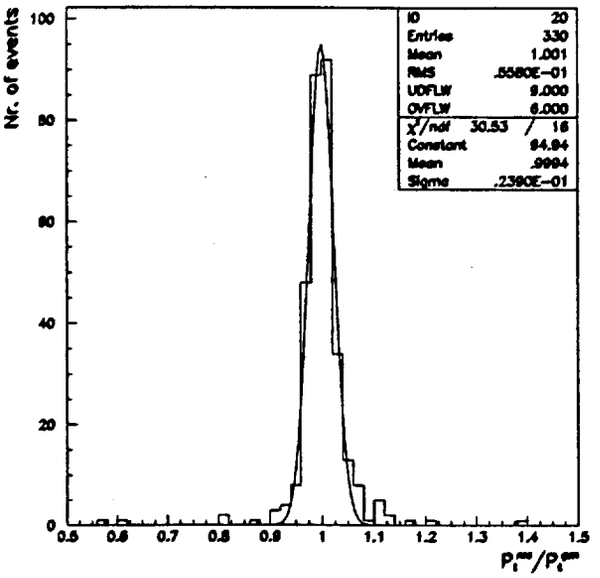

Figure 13: Transverse momentum resolution in the barrel region of the Panel lay-out.

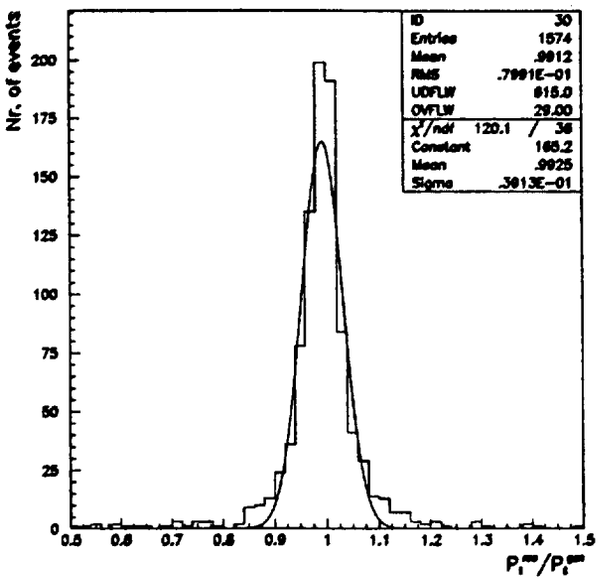

Figure 14: Transverse momentum resolution in the end-cap regions of the Panel lay-out.

is indicated also from the tails of the two distributions, which are much larger in the end-cap distribution. It is obvious from Figure 14 that almost 41% of the events are outside the histogram bounds, in comparison to Figure 13 where only 5% of the events lie outside these bounds.

6 Conclusions

Detailed studies have been made on the τ identification capabilities of the ATLAS Inner Tracker using fully simulated one- and three-prong single τ hadronic decays with both the Panel and Coseners House configurations and track reconstruction algorithms based on either both the TRT+SCT or only on the SCT subsystems. In addition, a comparison between the barrel and end-cap regions has been made from fully simulated $A^0 \rightarrow \tau\tau$ events.

The figures of merit we have considered are a) the track reconstruction efficiency, b) the fake track rate, c) the rate of charge misidentification, d) the transverse momentum resolution, e) the impact parameter and f) the τ decay vertex reconstruction.

7 Acknowledgements

We would like to thank Alan Poppleton and Igor Gavrilenko for the numerous discussions and for their help without which this work would not have been possible.

References

[1] GEANT Detector Description and Simulation Tool, CERN Program Library Q123.

[2] T. Sjostrand, CERN-TH.7111/93 and CERN/-TH.7112/93.

[3] ATLAS Software Group, DICE Manual, ATLAS Internal Note SOFT-NO-011 (1994)
M. Nessi *et. al.* ATLAS Internal Note SOFT-NO-016 (1994)
R. S. DeWolf, SLUG Manual, ATLAS Internal Note SOFT-NO-012 (1993).

[4] I. Gavrilenko, ATLAS Note INDET-NO-016, 21 October 1992.

[5] R. Clifft and A. Poppleton, ATLAS Note SOFT-NO-009, 14 June 1994.

[6] P. Billoir et al., DELPHI Note 86-99 PROG 61, November 1986.